Short-Time Velocity Identification and Coherent-Like Detection of Ultra-High Speed Targets

Jun Chen, Fei Wang, Jianjiang Zhou, *Member, IEEE*, Ling Li, Danny Crookes, *Senior Member, IEEE* and Huiyu Zhou

***Abstract*—Finding a balance between observation duration and detection rates is the ultimate goal of the detection of ultra high speed targets. However, short observation durations, both across range unit (ARU) and Doppler frequency migration (DFM), may severely limit the detection performance of ultra high speed targets. Although traditional coherent integration methods can efficiently accumulate signal energy to produce a high signal to noise ratio (SNR) measurement, they often need to search for unknown motion parameters. This search is time-consuming and unacceptable for real-time detection of ultra high speed targets. In this paper, a coherent-like detection method is designed based on the finite-dimension theory of Wigner matrices along with velocity identification. The proposed method can efficiently integrate signal energy without rendering motion parameters. We use the distribution and mean of the eigenvalues of the constructed matrix, i.e. an additive Wigner matrix, to identify velocities and detect ultra high speed targets, respectively. Simulation results validate the theoretical derivation, superiority and operability of the proposed method.**

***Index Terms*—Ultra high speed target, Wigner matrix, velocity identification, coherent integration, short observation time.**

I. Introduction

In modern battlefields, the speed of an aircraft plays a crucial role in achieving combat superiority. Many countries across the world strive to develop high speed aircraft, and consequently an increasing number of ultra high speed aircraft (normally with a velocity over Mach 5) are employed for long-range prompt strike and penetration [1], [2]. These high speed aircraft can severely threaten the detection capability of radar. Based on their velocity ranges, we can categorise existing aircraft into three types: hypersonic (Mach 5-10), high-hypersonic (Mach 10-25) and re-entry speed (> Mach 25). Since the velocity of an ultra high speed target cannot be ignored anymore in the estimation, compared with that of light, the echo is unable to match the transmitted signals and obtain sufficient high energy gains. Moreover, for pulse Doppler (PD) radar, ultra high speed aircraft echoes spread across several bins, which is called the across range unit (ARU) effect [3], [4]. During a short observation period, the Doppler shift is not a constant anymore and can be replaced by a non-linear higher order polynomial of slow-time. In other words, the time-varying Doppler may exceed the PD radar frequency resolution, which is known as the Doppler frequency migration (DFM) [3]. In the Doppler domain, the energy of a target is distributed over various ranges and frequency bins. It is difficult for a radar to accumulate signal energy and to detect the target using its motion states and the Doppler information of the target. Traditional coherent integration techniques are no longer applicable. It is challenging to design a robust and effective method to maintain the detection performance for ultra high speed targets in a short observation duration [5].

Research on the detection of ultra high speed aircraft has attracted increasing attention in recent years [5], [6], [36]. Unfortunately, research achievements in this area are very limited. In modern PD radar systems, target detection generally contains two energy integrations in the fast- and slow-time domains respectively [7]–[9]. Detecting ultra high speed targets follows the same principal. The first integration in the fast-time domain is through match filtering. However, for an ultra high speed target, the reference signal which is matched against the radar reflection is no longer the transmitted signal, whose phase should be modified according to the phase of the echoes of the target. Many studies have been conducted in the second integration for mitigating the ARU and DFM effects for regular speed maneuvering targets. These two issues severely degrade the system performance of detecting ultra high speed targets in regular circumstances. Based on the modulation information of echoes, the second integration practice is often divided into coherent integration and incoherent integration [7].

Coherent integration methods use additional phase information, resulting in higher integration gains than the incoherent integration methods. Classical coherent integration methods are based on a standard moving target detection (MTD) algorithm e.g. [10], [11], which can be implemented using a Fourier transform (FT) in each range bin. Unfortunately,

This work is supported by the National Natural Science Foundation of China (Grant No. 61371170), the Fundamental Research Funds for the Central Universities (Grant No. NP2015404, No. NS2016038), the Aeronautical Science Foundation of China (Grant No. 20152052028) and the Funding of Jiangsu Innovation Program for Graduate Education (Grant No. KYLX15_0282). H. Zhou is supported by UK EPSRC under Grant EP/N011074/1 and Royal Society-Newton Advanced Fellowship under Grant NA160342.

J. Chen, F. Wang and J. Zhou are with Key Laboratory of Radar Imaging and Microwave Photonics, Ministry of Education, Nanjing University of Aeronautics and Astronautics, Nanjing, 210016, China. E-mail: {junchen;wangxiaoxian;zjjee}@nuaa.edu.cn.

L. Li is with the University of Kent, United Kingdom. E-mail: C.Li@kent.ac.uk.

J. Chen and D. Crookes are with School of Electronics, Electrical Engineering and Computer Science, Queen's University Belfast, Belfast, United Kingdom. E-mail: {jon.chen;d.crookes}@qub.ac.uk.

H. Zhou is with Department of Informatics, University of Leicester, United Kingdom. E-mail: hz143@le.ac.uk.

Manuscript received 24 January, 2018; revised xxx.

MTD cannot solve problems such as ARU and DFM. Keystone transform (KT) [12], [13] and its variants demonstrated better performance in dealing with ARU and DFM. Yet, they still need certain prior information to handle Doppler ambiguity and these approaches are not effective for maneuvering targets and the detection of ultra high speed targets. Recently, Radon-Fourier transform (RFT) [14]–[16], Radon-fractional Fourier transform (RFrFT) [17], [18] and Radon-Lv's distribution (RLVD) [19], [20] have been proposed to deal with the ARU and DFM problems. RFrFT treats the Doppler frequency of a maneuvering target as a linear frequency modulation (LFM) signal, and uses the fractional Fourier transform (FrFT) [13], [21] to improve coherent integration gains instead of FT in the RFT algorithm. Like FrFT, Lv's distribution (LVD) is also a time-frequency analysis method, designed for LFM signals to integrate the energy in the centroid frequency-chirp rate domain. However, LVD outperforms FrFT on the detection of LFM signals, which results in superior detection performance by the coherent integration method RLVD. All of these algorithms need to define suitable motion parameters, which is time-consuming and inapplicable for real-time detection of ultra high speed targets.

On the other hand, incoherent integration methods do not need any prior information about the structure of the received signals, which makes this type of detection methods relatively easier to implement. Classical incoherent integration methods include maximum likelihood (ML) [22], [23] method, polynomial-phase transform (PPT) [24], Hough transform (HT) [25], Radon transform (RT) [26], and dynamic programming (DP) technology [27]. More recently, the track-before-detection (TBD) framework [28]–[30] was proposed for weak signal detection so as to further improve the signal to noise ratio (SNR). These incoherent detection methods can address the ARU and DFM effects in part or entirely. Nevertheless, most of these methods need to search for the unknown motion parameters, normally leading to high computational complexity.

Considering the requirements of computational complexity and accuracy for ultra high speed targets, motivated by the established methods, we here propose a coherent-like integration method using the finite-dimension random matrix theory [33], [34], which not only requires low computational complexity, but also can achieve better detection performance. The proposed method neither uses phase information of the echoes nor needs to search for motion parameters. The proposed method stems from the same theory of a coherent integration method. A standard coherent integration method performs cancellation of background noise to achieve the improvement of SNR. Comparably, our designed method utilizes the eigenvalues of Wigner matrices [31]–[34] (a classical random matrix) to capture high speed targets. In other words, we undertake eigenvalue based cancellation of background noise in order to improve SNR. Besides, the existence of ultra high speed targets can seriously disturb the spectral distribution of Wigner matrices, compared with that of low speed targets. The difference of interference degrees can be utilized to identify the velocity range of the detected target, which can be measured by the Kullback-Leibler divergence (KLD) [35] between different spectral distributions of multiple velocities.

The rest of this paper is organized as follows. In Section II, we introduce preliminaries about Wigner matrices to facilitate the understanding of the proposed identification and detection method. In Section III, the echo model of an ultra high speed target is introduced and analyzed. In Section IV, an identification method of ultra high speed targets based on Wigner matrices is proposed. We here present the proposed method in detail and the establishment of identification thresholds for different velocities. In Section V, an eigenvalue based detection method for ultra high speed targets is designed, while the technical details and the computational complexity of the proposed method are also discussed. Both the theoretical and experimental justification of the proposed method are reported in Section VI. Section VII concludes this paper.

II. Preliminaries

In probability theory and mathematical physics, random matrices play an important role in the fields of telecommunication, physics, control, and finance. As an important element, Wigner matrices have been widely used in recent years. They follow a recognised limiting spectral distribution (LSD) law that is homogeneous to the semi-circular law [31], [32].

Definition 1 (Wigner matrix)**.** *An $n \times n$ Hermitian matrix $\boldsymbol{W}_n$ is a Wigner matrix if its off-diagonal entries are independent and identically distributed (IID) complex random variables with zero mean and $\sigma^2 = 1$ variance, and the diagonal entries are IID real random variables.*

Lemma 1 (Semi-circular law)**.** *As $n \to \infty$, the empirical spectral distribution of the normalized Wigner matrix $\frac{1}{\sqrt{n}}\boldsymbol{W}_n$ converges weakly to the semi-circular law with the density:*

$$f^{\frac{1}{\sqrt{n}}\boldsymbol{W}_n}(x) = \frac{1}{2\pi}\sqrt{4-x^2}\ \mathbf{1}_{[-2,2]}(x). \tag{1}$$

III. The Echo Model of Ultra High Speed Targets

To effectively detect a target via PD radar, the transmission by radar is a narrow-band linear frequency modulated (LFM) signal, which is treated as a point target on radar. The transmitted signal of the PD radar can be denoted as:

$$\begin{aligned} s(t) = \sum_m \Bigg\{ &\mathrm{rect}\left(\frac{t-mT_I}{T_P}\right)\cdot \exp\left\{j2\pi f_c t\right\} \\ &\cdot\exp\left\{j\pi k\left(t-mT_I\right)^2\right\}\Bigg\}, \end{aligned} \tag{2}$$

where, $\mathrm{rect}(x)$ is a gate function,

$$\mathrm{rect}(x) = \begin{cases} 1, & |x| \le \frac{1}{2} \\ 0, & |x| > \frac{1}{2} \end{cases} \tag{3}$$

where m represents the pulse sequence number, T_I denotes the pulse repetition interval (PRI) of the radar system, T_P denotes the pulse duration, f_c is the radar carrier frequency, and $k = \frac{B}{T_P}$ is the frequency modulated rate with bandwidth B. Here, t is the fast-time.

After the demodulation, the echo signals from the point target can be written as follows:

$$s_r(t) = A_t \cdot \sum_m \left\{ \text{rect}\left(\alpha \frac{t-\tau-mT_I}{T_P}\right) \cdot \exp\{-j2\pi f_c \alpha \tau\} \cdot \exp\left\{j\pi k\alpha^2 (t-\tau-mT_I)^2\right\}\right\}, \tag{4}$$

where $\alpha = \frac{c-v(t_m)}{c+v(t_m)}$, $\tau = \frac{2r(t_m)}{c-v(t_m)}$ is the time delay in which $v(t_m)$ and $r(t_m)$ are the instantaneous velocity and the instantaneous distance between the target and the radar, t_m is the slow-time, and c is the velocity of light. A_t represents the fluctuant change of the echo amplitudes. For a low speed target, since the instantaneous velocity $v(t_m)$ is much less than the velocity of light c, $\alpha \approx 1$ and $\tau \approx \frac{2r(t_m)}{c}$. However, for an ultra high speed target, the instantaneous velocity $v(t_m)$ of the target cannot be ignored in the calculation of α and τ.

For an ultra high speed target, since the velocity $v(t)$ of the target cannot be ignored, compared against the velocity of light, the matched filter is no longer $u^{\mathrm{H}}(-t)$ but $u^{\mathrm{H}}(-\alpha t)$, where $u(t) = \text{rect}\left(\frac{t}{T_P}\right)\exp\{j\pi k t^2\}$, and u^{H} denotes the conjugate transpose of u. When the velocity and acceleration satisfy the following relationship [36]:

$$|v|T_P < \frac{c}{2B} \quad \text{or} \quad a < \frac{\lambda B}{T_P(2+BT_P)}, \tag{5}$$

where a is the acceleration of the target and λ is the wavelength, we can also use $u^{\mathrm{H}}(-t)$ as the matched filter.

The echo signal $s_{MF}(t)$ after the matched filtering is

$$s_{MF}(t) = A_0 \text{sinc}[B(t-\tau)] \exp\{-j2\pi f_c \alpha \tau\}, \tag{6}$$

where, A_0 is the amplitude of the echo after the matched filtering.

According to Eq. (6), the Doppler frequency of the ultra-high speed target can be calculated as

$$\begin{aligned} f_d &= \frac{f_c \mathrm{d}(\alpha\tau)}{\mathrm{d}t_m} = \frac{f_c \mathrm{d}\left(\frac{2r(t_m)}{c+v(t_m)}\right)}{\mathrm{d}t_m} \\ &= \frac{2f_c \mathrm{d}r(t_m)}{[c+v(t_m)]\,\mathrm{d}t_m} - \frac{2f_c r(t_m)\,\mathrm{d}v(t_m)}{[c+v(t_m)]^2\,\mathrm{d}t_m}, \end{aligned} \tag{7}$$

where, the instantaneous distance $r(t_m)$ can be expressed as the Taylor series expansion,

$$r(t_m) = r_0 + \sum_{k=1}^{\infty}\left[\frac{r^{(k)}(0)}{k!}t_m^k\right] \approx r_0 + \sum_{k=1}^{K}\left[\frac{r^{(k)}(0)}{k!}t_m^k\right], \tag{8}$$

where, r_0 is the initial range between the target and the radar, $r^{(k)}(0)$ denotes the k-order derivative of $r(t_m)$ at $t_m = 0$. Since the instantaneous distance $r(t_m)$ of the ultra-high speed target should contain not only the term of range migration, but also the higher order term of range curvature, we usually use $K = 3$ to describe the ultra-high speed target. Then, the instantaneous radial velocity $v(t_m)$ can be computed as

$$v(t_m) = \frac{\mathrm{d}r(t_m)}{\mathrm{d}t_m} = \sum_{k=1}^{K}\left[\frac{r^{(k)}(0)}{(k-1)!}t_m^{k-1}\right]. \tag{9}$$

According to Eqs. (8) and (9), the first term of the right hand side of Eq. (7) can be expressed as

$$\begin{aligned} \frac{2f_c \mathrm{d}r(t_m)}{[c+v(t_m)]\,\mathrm{d}t_m} &= \frac{2f_c v(t_m)}{c+v(t_m)} = 2f_c - \frac{2f_c c}{c+v(t_m)} \\ &= 2f_c - \frac{2f_c c}{c+\sum_{k=1}^{K}\left[\frac{r^{(k)}(0)}{(k-1)!}t_m^{k-1}\right]}, \end{aligned} \tag{10}$$

and the second term of the right hand side of Eq. (7) can be expressed as

$$\begin{aligned} \frac{2f_c r(t_m)\,\mathrm{d}v(t_m)}{[c+v(t_m)]^2\,\mathrm{d}t_m} &= \frac{2f_c r(t_m)\sum_{k=2}^{K}\left[\frac{r^{(k)}(0)}{(k-2)!}t_m^{k-2}\right]}{[c+v(t_m)]^2} \\ &= \frac{2f_c\left(r_0+\sum_{k=1}^{K}\left[\frac{r^{(k)}(0)}{k!}t_m^k\right]\right)\sum_{k=2}^{K}\left[\frac{r^{(k)}(0)}{(k-2)!}t_m^{k-2}\right]}{\left[c+\sum_{k=1}^{K}\left[\frac{r^{(k)}(0)}{(k-1)!}t_m^{k-1}\right]\right]^2}. \end{aligned} \tag{11}$$

The exponents of the numerator and the denominator in Eq. (11) are the same, both of which are $2K-2$, and the first term of the right hand side of Eq. (7) which is shown in Eq. (10) has the form of an inverse proportional function of slow-time. The Doppler frequency of the ultra-high speed target expressed in Eq. (7) is no longer a linear function of slow-time. Therefore, the target detection methods, based on the assumption that the Doppler frequency is LFM, are not suitable for ultra-high speed targets anymore.

IV. Identification of Ultra-High Speed Targets

Since ultra-high speed targets have a higher velocity than regular military targets, we cannot use those systems designed for low- and mid-velocity targets; so we have to propose a new method to detect and identify high speed targets. In this section, we will propose an easy and effective method to identify them by using the spectral property of Wigner matrices in finite dimensions.

A. Identification Theory

Suppose that both low speed and ultra-high speed targets, which presumably have the same Radar Cross-Section (RCS) [37], exist in each pulse during a short observation time. After demodulation and matched filtering which are introduced in Section III, these targets very likely hold very similar energy in the received data. Thus, it is very difficult to identify them using energy estimation. Due to the short observation time and ultra high speeds, the energy in each range bin is relatively low, and consequently the Doppler information is hard to be extracted. Therefore, the echoes of the ultra high speed targets accompany the problem of Doppler ambiguity. Here, we will identify them using the difference of the numbers of the range bins instead of the Doppler maps.

Assume that the number of the engaged range bins of a low speed target is denoted as P, and the number of the involved range bins of an ultra high speed target is denoted as K, where the difference between them satisfies $\Delta_r = K - P > 0$ during a short observation time T_O. The received sampling data can be constructed as a two-dimensional matrix $\mathbf{R}$ in a range and slow-time domain. The number of the rows of the matrix $\mathbf{R}$

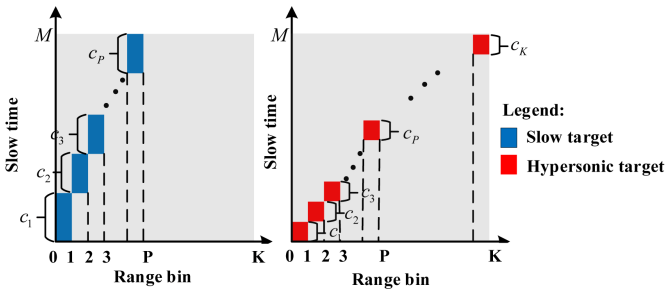

Fig. 1. Illustration of the range bin where the target exists in each pulse.

is the observed number of PRI, which can be calculated as $M = \lfloor \frac{T_O}{T_I} \rfloor$. Without loss of generality, we let the target move along an initial observation distance and exist within the whole short observation time. We choose the first K range bins for testing, allowing the echo of an ultra high speed target to appear in the test matrix.

The target energy can be gathered in one range bin effectively after the matched filtering and the target energy in the other range bins has little effect on the identification results. For the simplicity of the theoretical derivation, we ignore the target energy in the other range bins. The two-dimension matrix $\mathbf{R}$, whose size is $M \times K$, is illustrated in Fig. 1. Therein, we denote the number of pulses where the target exists in the k^{th} range bin as c_k, which satisfies the following condition:

$$\begin{cases} \text{for low speed targets:} \\ c_1 + c_2 + \cdots + c_P = M; c_{P+1} = \cdots = c_K = 0 \\ \text{for ultra high speed targets:} \\ c_1 + c_2 + \cdots + c_K = M \end{cases}. \tag{12}$$

Then, the two-dimensional matrix $\mathbf{R}_{M\times K}$ for testing can be expressed as:

$$\begin{aligned} &\mathbf{R}_{M\times K} = (r_{ij})_{i=1,j=1}^{M,K} \\ &= \begin{cases} \eta_{ij} + n_{ij} & ,i \in \mathbf{C}_k, \mathbf{C}_k \neq \emptyset, j = k, k = 1, 2, \cdots, K \\ n_{ij} & ,others \end{cases}, \end{aligned} \tag{13}$$

where $\mathbf{C}_k$ is the set of the serial numbers of the row in which the target signal exists in the k^{th} range bin. It can be calculated as:

$$\mathbf{C}_k = \begin{cases} \{\Delta_{k-1} + 1, \cdots, \Delta_{k-1} + c_k\} & ,\Delta_k > \Delta_{k-1} \\ \emptyset & ,\Delta_k = \Delta_{k-1} \end{cases}, \tag{14}$$

wherein $\Delta_k = \sum_{i=1}^{k} c_i$ and $\Delta_0 = 0$, n_{ij} are IID random variables drawn from a standard normal distribution. Since the observation time is very short, the velocity of the target can be regarded as a constant. We can use the same value η to represent the gathered energy η_{ij} in each pulse after the matched filtering.

The sample covariance matrix of $\mathbf{R}_{M\times K}$ can be calculated as:

$$\Phi_{\mathbf{R}} = \frac{1}{M-1}\mathbf{R}^T\mathbf{R} = \Phi_{\mathbf{N}} + \Phi_{\mathbf{S}} + \Phi_{\mathbf{N,S}}, \tag{15}$$

where the symbol $(\cdot)^T$ denotes the transpose, $\Phi_{\mathbf{N}}$ is the noise component after the matched filtering, $\Phi_{\mathbf{N,S}}$ is a cross term related to the target and noise, and the component $\Phi_{\mathbf{S}}$ which contains the target information is:

$$\Phi_{\mathbf{S}} = diag\left\{\frac{c_1\eta^2}{M-1}, \frac{c_2\eta^2}{M-1}, \cdots, \frac{c_K\eta^2}{M-1}\right\}. \tag{16}$$

In practice, after the matched filtering, the elements of the noise component $\Phi_{\mathbf{N}}$ are correlated. Here, an additional decorrelation technique can be adopted to remove the correlation between the elements of $\Phi_{\mathbf{N}}$, e.g. [41]. The sample covariance matrix $\Phi_{\mathbf{R}}$ can be recast as:

$$\Phi_{\mathbf{R}}^{\dagger} = \mathbf{Q}^{-1}\Phi_{\mathbf{N}}\mathbf{Q}^{-1} + \mathbf{Q}^{-1}\left(\Phi_{\mathbf{S}} + \Phi_{\mathbf{N,S}}\right)\mathbf{Q}^{-1} = \Phi_{\mathbf{N}}^{\dagger} + \Phi_{\mathbf{S}}^{\dagger}, \tag{17}$$

where $\mathbf{Q} = \mathrm{E}\left[\mathbf{n}_r\mathbf{n}_r^T\right]$, $\mathbf{n}_r$ is a $K \times 1$ output vector of the matched filter whose input is a white Gaussian noise vector, and $(\cdot)^{-1}$ denotes matrix inversion.

As $M \to \infty$ (usually $M \geq 100$), we have $\Phi_{\mathbf{N}}^{\dagger} \to \mathbf{I}_K$, where $\mathbf{I}_K$ is the $K \times K$ identity matrix, and $\sqrt{M}\left(\Phi_{\mathbf{N}}^{\dagger} - \mathbf{I}_K\right)$ as Φ_W, which is a Wigner matrix. Thus, the sample covariance matrix $\Phi_{\mathbf{R}}^{\dagger}$ can be reconstructed as follows:

$$\widetilde{\Phi}_{\mathbf{R}} = \sqrt{M}\left(\Phi_{\mathbf{R}}^{\dagger} - \mathbf{I}_K\right) = \Phi_W + \widetilde{\Phi}_{\mathbf{S}}, \tag{18}$$

where

$$\widetilde{\Phi}_{\mathbf{S}} = \sqrt{M}\Phi_{\mathbf{S}}^{\dagger} = \sqrt{M}\mathbf{Q}^{-1}\left(\Phi_{\mathbf{S}} + \Phi_{\mathbf{N,S}}\right)\mathbf{Q}^{-1}. \tag{19}$$

Since Φ_W is a random matrix, $\widetilde{\Phi}_{\mathbf{R}}$ is naturally a random matrix. We denote the eigenvalues and eigenvectors of matrix $\widetilde{\Phi}_{\mathbf{R}}$ as $\widetilde{\lambda}_k$ and $\widetilde{\varphi}^{\widetilde{\lambda}_k}$, $k = 1, 2, \cdots, K$, where the eigenvalue $\widetilde{\lambda}_k$ can be treated as a random variable with probability density function (PDF) $\widetilde{f}_k(\lambda)$. As a result, we have:

$$\sum_{k=1}^{K}\widetilde{\Phi}_{\mathbf{R}}(h,k)\,\widetilde{\varphi}^{\widetilde{\lambda}_h}(k) = \widetilde{\lambda}_h\widetilde{\varphi}^{\widetilde{\lambda}_h}(h). \tag{20}$$

When $\widetilde{\varphi}^{\widetilde{\lambda}_h}(h) \neq 0$, Eq. (20) can be recast as:

$$\sum_{k=1,k\neq h}^{K}\widetilde{\Phi}_{\mathbf{R}}(h,k)\frac{\widetilde{\varphi}^{\widetilde{\lambda}_h}(k)}{\widetilde{\varphi}^{\widetilde{\lambda}_h}(h)} + \widetilde{\Phi}_{\mathbf{R}}(h,h) = \widetilde{\lambda}_h. \tag{21}$$

We denote $\frac{\widetilde{\varphi}^{\widetilde{\lambda}_h}(k)}{\widetilde{\varphi}^{\widetilde{\lambda}_h}(h)}$ by $b(h,k)$, and Eq. (21) can be written as:

$$\sum_{k=1,k\neq h}^{K}\widetilde{\Phi}_{\mathbf{R}}(h,k)\,b(h,k) + \widetilde{\Phi}_{\mathbf{R}}(h,h) = \widetilde{\lambda}_h. \tag{22}$$

According to Eqs. (18) and (19), matrix $\widetilde{\Phi}_{\mathbf{S}}$ can be approximated to a diagonal matrix, so we have:

$$\widetilde{\Phi}_{\mathbf{R}}(h,k) = \begin{cases} \Phi_W(h,k) & ,k \neq h \\ \Phi_W(h,h) + \widetilde{\Phi}_{\mathbf{S}}(h,h) & ,k = h \end{cases}. \tag{23}$$

Therefore, Eq. (22) can be written as:

$$\sum_{k=1,k\neq h}^{K}\Phi_W(h,k)\,b(h,k) + \Phi_W(h,h) = \widetilde{\lambda}_h - \widetilde{\Phi}_{\mathbf{S}}(h,h). \tag{24}$$

Comparing Eq. (24) with (22), since $\widetilde{\lambda}_h$ are the eigenvalues of matrix $\widetilde{\Phi}_{\mathbf{R}}$ shown in Eq. (22), we recognise that $\lambda_h = \widetilde{\lambda}_h - \widetilde{\Phi}_{\mathbf{S}}(h,h)$, where $h = 1, \cdots, K$ are the eigenvalues of

Wigner matrix Φ_W, whose PDF can be denoted by $f_h(\lambda)$, and the global PDF $f(\lambda)$ of these eigenvalues is [34]:

$$f(\lambda)=\frac{1}{K}\sum_{i=0}^{K-2}h_i^2(\lambda)+\frac{1}{2K}h_{K-1}^2(\lambda). \tag{25}$$

where K is even and $h_i(x)$ is the normalized Hermite function, which can be written as $h_i(x)=\left(\sqrt{\pi}\cdot 2^i\right)^{-\frac{1}{2}}\cdot(i!)^{\frac{1}{2}}\cdot e^{-\frac{1}{2}x^2}\cdot\sum_{l=0}^{\lfloor\frac{i}{2}\rfloor}\left[\frac{(-1)^l}{l!(i-2l)!}(2x)^{i-2l}\right]$.

Thus, the PDFs of random variable $\widetilde{\lambda}_h$, where $h=1,2,\cdots,K$, are shown below:

$$\widetilde{f}_h(\lambda)=f_h\left(\lambda-\widetilde{\Phi}_{\mathbf{S}}(h,h)\right), \tag{26}$$

and we denote the global PDF of eigenvalues $\widetilde{\lambda}_h$, $h=1,2,\cdots,K$, as $\widetilde{f}(\lambda)$. The difference between $\widetilde{f}(\lambda)$ and $f(\lambda)$ can be used to identify the targets with different velocities. Proposition 1 states mathematically that there must be a difference between the two PDFs, when the target exists.

Proposition 1 (Identification principle)**.** *Let $\lambda(h,\zeta),h=1,2,\cdots,K$ be random variables from a random process $\lambda(\zeta)$, each of which is of PDF $\widetilde{f}_h(\lambda,\theta_h)$, where $\theta_h=\widetilde{\Phi}_{\boldsymbol{S}}(h,h)$. For a fixed ζ, we have PDF $\widetilde{f}(\lambda)$, based on the samples $\lambda(h,\zeta),h=1,2,\cdots,K$, is not equal to $f(\lambda)$.*

Proof: For a fixed ζ, the cumulative distribution function (CDF) based on the samples $\lambda(h,\zeta),h=1,2,\cdots,K$ can be expressed as follows:

$$F(\lambda|\zeta)=\frac{\sum_{h=1}^{K}I(\lambda(h,\zeta)\le\lambda)}{K}, \tag{27}$$

where $I(\cdot)$ is an indicator function.

The expectation of $F(\lambda|\zeta)$ for variable ζ is:

$$\begin{aligned}E\left[F(\lambda|\zeta)\right]&\approx\frac{\sum_{h=1}^{K}E\left[I(\lambda(h,\zeta)\le\lambda)\right]}{K}\\&=\frac{\sum_{h=1}^{K}\left[\int_{-\infty}^{\lambda}\widetilde{f}_h(x,\theta_h)\,\mathrm{d}x\right]}{K}=\frac{\int_{-\infty}^{\lambda}\left[\sum_{h=1}^{K}\widetilde{f}_h(x,\theta_h)\right]\mathrm{d}x}{K},\end{aligned} \tag{28}$$

where $E\left[F(\lambda|\zeta)\right]=\int_{-\infty}^{\lambda}f(x)\mathrm{d}x$ if and only if $\theta_1=\theta_2=\cdots=\theta_K=0$.

When the target exists, the parameters $\theta_h,h=1,\cdots,K$ are not equal or satisfy $\theta_1=\theta_2=\cdots=\theta_K\neq 0$. Thus, we reach the conclusion that, for a fixed ζ, the PDF $\widetilde{f}(\lambda)$ based on the samples $\lambda(h,\zeta),h=1,2,\cdots,K$ is not equal to $f(\lambda)$. ■

According to Proposition 1, we can use the difference between $\widetilde{f}(\lambda)$ and $f(\lambda)$ to identify the targets with different velocities. Here, KLD is used to measure the difference between these two PDFs, used as the identification criterion. The next subsection presents its computation method and its null and alternative distributions in more detail.

B. Determining Identification Thresholds

Since the interval of the eigenvalues of matrix $\widetilde{\Phi}_{\mathbf{R}}$ is indeterminate, for the convenience of the numerical KLD calculation, the probability integral transform (PIT) can be used here to transform the eigenvalues to the interval $[0,1]$. After we use the PIT $\widehat{\lambda}_h=F\left(\widetilde{\lambda}_h\right)$, the original eigenvalues can be transformed into an equivalent set $\widehat{\Lambda}=\left\{\widehat{\lambda}_h,h=1,2,\cdots,K\right\}$, where, the CDF $F(\lambda)$ of the Wigner matrix in a finite dimension is [33]:

$$\begin{aligned}F(\lambda)=&\frac{1}{K}\int_{-\infty}^{\lambda}h_0^2(x)\,\mathrm{d}x+\frac{1}{K}\int_{-\infty}^{\lambda}h_1^2(x)\,\mathrm{d}x\\&+\frac{1}{K}\sum_{i=2}^{K-2}\left[\frac{1}{\sqrt{\pi}\cdot 2^i\cdot i!}\cdot C_i(\lambda)+\Phi\left(\sqrt{2}\lambda\right)\right]\\&+\frac{1}{2K}\left[\frac{C_{K-1}(\lambda)}{\sqrt{\pi}\cdot 2^{K-1}\cdot(K-1)!}+\Phi\left(\sqrt{2}\lambda\right)\right],\end{aligned} \tag{29}$$

where:

$$\begin{aligned}C_i(x)=&-e^{-x^2}H_i(x)H_{i-1}(x)+(-1)^i e^{-x^2}\sum_{t=1}^{i-1}\left\{(-1)^t\cdot\right.\\&\left.2^t\cdot\left[\prod_{s=0}^{t-1}(i-s)\right]\cdot(-1)^{i-t-1}\cdot H_{i-t}(x)\cdot H_{i-t-1}(x)\right\},\end{aligned} \tag{30}$$

and $H_i(x)=i!\sum_{l=0}^{\lfloor\frac{i}{2}\rfloor}\frac{(-1)^l}{l!(i-2l)!}(2x)^{i-2l}$.

If a high speed target does not exist in the scene, the entries of set $\widehat{\Lambda}$ come from the uniform distribution $\mathrm{U}[0,1]$. Therefore, since set $\Lambda=\left\{\widetilde{\lambda}_h,h=1,2,\cdots,K\right\}\Rightarrow\widehat{\Lambda}$, $\widetilde{F}(x)\Rightarrow\widetilde{U}(x)=\frac{1}{K}\#\left\{h\le K:\widehat{\lambda}_h\le x\right\}$, where $\Rightarrow$ denotes the mapping, $\#$ denotes the cardinality of the set, and $\widetilde{F}(x)$ is the CDF of PDF $\widetilde{f}(x)$ based on the samples $\widetilde{\lambda}_h,h=1,2,\cdots,K$. Now, we calculate the KLD between the CDF $\widetilde{U}(x)$ and the uniform distribution $\mathrm{U}[0,1]$ to measure the difference between $\widetilde{f}(\lambda)$ and $f(\lambda)$, which is the identification criterion.

We denote u_t, where $t=0,1,\cdots,T$, as the equally spaced partition points in the interval $[0,1]$ [39], and $0=u_0<u_1<\cdots<u_T=1$. The KLD can be numerically recast as:

$$D_{KL}\approx\log T+\sum_{t=1}^{T}\frac{\widetilde{U}(u_t)-\widetilde{U}(u_{t-1})}{K}\log\frac{\widetilde{U}(u_t)-\widetilde{U}(u_{t-1})}{K}. \tag{31}$$

The calculation procedure for estimating D_{KL} is illustrated in Fig. 2.

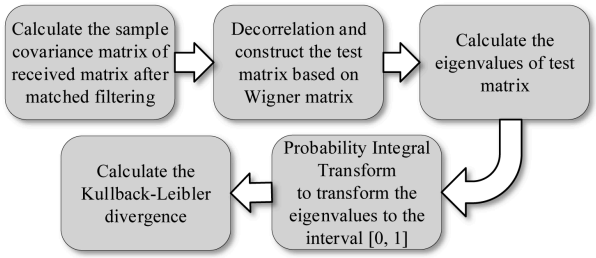

Fig. 2. Detailed calculation procedure for estimating D_{KL}.

Next, we will derive the null and alternative distributions of the identification criterion D_{KL} respectively to obtain the

identification threshold, identification probability and corresponding false identification rate.

Firstly, we specify the null distribution of D_{KL}. When a target does not exist in the scene, the relationship between D_{KL} and G tests is $D_{KL}=\frac{G}{2K}$, and the relationship between G and χ^2 tests is $G\approx X^2$. Thus, we have $D_{KL}=\frac{1}{2K}X^2$. Since X^2 has a χ^2 distribution with $T-1$ degrees of freedom, the characteristic function of the χ^2_{T-1} distribution is $\Phi_{X^2}(t)=(1-2it)^{-\frac{T-1}{2}}$. According to the linear relationship between X^2 and D_{KL}, the characteristic function of D_{KL} is

$$\Phi_{D_{KL}}(t)=\Phi_{X^2}(\frac{1}{2K}t)=\left(1-\frac{it}{K}\right)^{-\frac{T-1}{2}}, \tag{32}$$

which is the characteristic function of a gamma distribution with the shape parameter $\mu=\frac{T-1}{2}$ and the scale parameter $\theta=\frac{1}{K}$. Thus, the CDF of D_{KL} with no target can be expressed as follows:

$$F_0\left(x,\mu,\theta\right)=\frac{1}{\Gamma\left(\mu\right)}\gamma\left(\mu,\frac{x}{\theta}\right), \tag{33}$$

where $\Gamma\left(\cdot\right)$ is a complete gamma function, and $\gamma\left(\cdot\right)$ is the lower incomplete Gamma function.

Then, we consider the expression of the alternative distribution of D_{KL} by utilizing a chi-squared test.

We first calculate the theoretical probability distribution of the eigenvalues which contain a high speed target. Based on Eq. (29), we have $\widetilde{u}_t=F^{-1}\left(u_t\right)$, that is $F\left(\widetilde{u}_t\right)-F\left(\widetilde{u}_{t-1}\right)=\frac{1}{T}$, $t=1,2,\cdots,T$, where $F^{-1}(\cdot)$ is the inverse function of $F(\cdot)$. We define $P_t=\widetilde{F}\left(\widetilde{u}_t\right)-\widetilde{F}\left(\widetilde{u}_{t-1}\right)$, $t=1,2,\cdots,T-1$, where, $\widetilde{F}(\cdot)$ is the CDF of $\widetilde{f}(\cdot)$, and $P_T=1-\widetilde{F}\left(\widetilde{u}_{T-1}\right)$. Thus, the theoretical probability distribution, after PIT has been performed, is:

$$\widetilde{P}_t=\frac{P\cdot P_t}{K}+\frac{K-P}{K\cdot T}, \tag{34}$$

where, for an ultra-high speed target, $P=K$, and for another velocity v, $P=\lceil\frac{vT_O}{\Delta_r}\rceil$, where, Δ_r is the range resolution.

Then, through introducing the theoretical probability distribution $\widetilde{P}_t$ to the calculation of KLD, and denoting $\frac{\widetilde{U}(u_t)-\widetilde{U}(u_{t-1})}{K}$ by $\widehat{P}_t$, the KLD in Eq. (31) can be recast as:

$$\begin{aligned}D_{KL}&=\log T+\sum_{t=1}^{T}\widehat{P}_t\log\widehat{P}_t\\&=\sum_{t=1}^{T}\widehat{P}_t\log\frac{\widehat{P}_t}{\widetilde{P}_t}+\sum_{t=1}^{T}\left(\widehat{P}_t-\widetilde{P}_t\right)\log\widetilde{P}_t+C\left(v,\Phi_{\mathbf{S}}\right),\end{aligned} \tag{35}$$

where $C\left(v,\Phi_{\mathbf{S}}\right)$ is a function of target velocity v and target component $\Phi_{\mathbf{S}}$, which can be computed as:

$$C\left(v,\Phi_{\mathbf{S}}\right)=\sum_{t=1}^{T}\widetilde{P}_t\log\widetilde{P}_t+\log T, \tag{36}$$

where, by substituting the specific form of P and P_t into Eq. (34), the theoretical probability distribution $\widetilde{P}_t$ is

$$\widetilde{P}_t=\frac{\lceil\frac{vT_O}{\Delta_r}\rceil\left[\widetilde{F}\left(\widetilde{u}_t\right)-\widetilde{F}\left(\widetilde{u}_{t-1}\right)\right]T+K-\lceil\frac{vT_O}{\Delta_r}\rceil}{KT}. \tag{37}$$

By using the Taylor expansion, the numerical KLD in Eq. (35) can be written as:

$$\begin{aligned}D_{KL}&=E\left[\widehat{P}_t-\widetilde{P}_t\right]+\sum_{t=1}^{T}\frac{\left(\widetilde{P}_t-\widehat{P}_t\right)^2}{2\widehat{P}_t}+C\left(v,\Phi_{\mathbf{S}}\right)\\&=\sum_{t=1}^{T}\frac{\left(\widetilde{P}_t-\widehat{P}_t\right)^2}{2\widehat{P}_t}+C\left(v,\Phi_{\mathbf{S}}\right)=\frac{1}{2K}X^2+C\left(v,\Phi_{\mathbf{S}}\right).\end{aligned} \tag{38}$$

Since $\frac{1}{2K}X^2$ has a Gamma distribution $Gam\left(\frac{T-1}{2},\frac{1}{K}\right)$, the CDF of D_{KL} with a target is

$$F_I\left(x,v,\mu,\theta\right)=\frac{1}{\Gamma\left(\mu\right)}\gamma\left(\mu,\frac{x-C}{\theta}\right),\quad x>C, \tag{39}$$

where $\mu=\frac{T-1}{2}$, $\theta=\frac{1}{K}$, and $C\left(v,\Phi_{\mathbf{S}}\right)$ is denoted by C.

According to the null and alternative distributions $F_0\left(\cdot\right)$ and $F_I\left(\cdot\right)$, we can determine the identification threshold β_I, the identification probability $P_d\left(\cdot\right)$ and the false identification rate P_{fi}.

Assume the identification velocity is v_d. The identification threshold β_I with the false alarm rate P^1_{fa} is:

$$\beta_I=F_0^{-1}\left(1-P^1_{fa},\frac{T-1}{2},\frac{1}{K}\right)\Big|_{K=\lceil\frac{v_dT_O}{\Delta_r}\rceil}, \tag{40}$$

Using the identification threshold β_I, the identification probability of the ultra high speed target with velocity v_d can be calculated as:

$$P_d=1-F_I\left(\beta_I,v_d,\frac{T-1}{2},\frac{1}{K}\right)\Big|_{K=\lceil\frac{v_dT_O}{\Delta_r}\rceil}. \tag{41}$$

Under the identification threshold β_I, the detection probability of velocity v_{th}, which is called the false identification rate, can be written as:

$$P^{v_{th}}_{fi}=1-F_I\left(\beta_I,v_{th},\frac{T-1}{2},\frac{1}{K}\right)\Big|_{K=\lceil\frac{v_dT_O}{\Delta_r}\rceil}. \tag{42}$$

V. Proposed Detection Method of an Ultra-High Speed Target

A. Eigenvalue based Detection

As we know, the integration of different pulses can help significantly to improve the target detection performance. MTD is a traditional technique, which has two shortcomings for detecting high-speed maneuvering targets, i.e. across range unit (ARU) and Doppler frequency migration (DFM). In order to handle these problems, Xiaolong proposed Radon-Fractional-Fourier transform (RFrFT), which treats the Doppler frequency of a maneuvering target as a LFM signal and uses the FrFT to increase coherent integration gains after having followed the target trajectory [17]. However, this method needs to estimate the motion parameters, sacrificing efficiency that makes it unsuitable for short-time detection. In this section, we propose an eigenvalue based short-time integration method. It stems from a standard coherent integration method but has significant

innovations. The proposed method does not use the phase information of the echoes. Instead, it uses the zero expectation of the eigenvalues of a Wigner matrix to cancel the background noise, similar to the standard coherent integration method.

To accurately detect a target, we need to concentrate on the target energy and reduce the noise energy as much as possible. As shown in Eq. (16), the sum of the diagonal elements of matrix Φ_S can effectively accumulate the target energy, which can be written as:

$$\widetilde{Z_S} = (M-1)\sum_{h=1}^{K}\Phi_{\mathbf{S}}(h,h). \tag{43}$$

After decorrelation and reconstruction of matrix $\Phi_{\mathbf{R}}$, the accumulation of the target energy can be obtained by:

$$Z_S = \alpha\sum_{h=1}^{K}\left(\widetilde{\lambda}_h - \lambda_h\right), \tag{44}$$

where $\alpha = \frac{(M-1)}{\sqrt{M}}$.

The target detection problem can be formulated as a binary hypothesis test: $\mathcal{H}_1: \ Z_R = Z_S + Z_W$, $\mathcal{H}_0: \ Z_R = Z_W$, where $Z_W = \alpha\sum_{h=1}^{K}\lambda_h$.

According to the central limit theorem, when the sample size K is large (usually $K \geq 20$), whilst satisfying a practical radar target detection situation, $Z_R|\mathcal{H}_0$ closely simulates the normal distribution with mean $\alpha K\mu_0$ and standard deviation $\sigma = \alpha\sqrt{K}\sigma_0$, where μ_0 and σ_0 are the mean and standard deviation of the eigenvalues of Wigner matrix Φ_W.

Mean μ_0: According to Eq. (25), the mean must be 0, i.e. $\mu_0 = E[\lambda] = 0$.

Variance:

$$\begin{aligned}\sigma_0^2 &= Var[\lambda] = \int_{-a}^{a}\lambda^2 f(\lambda)\,\mathrm{d}\lambda \\ &= \frac{1}{K}\sum_{i=0}^{K-2}\int_{-a}^{a}\lambda^2 h_i^2(\lambda)\,\mathrm{d}\lambda + \frac{1}{2K}\int_{-a}^{a}\lambda^2 h_{K-1}^2(\lambda)\,\mathrm{d}\lambda,\end{aligned} \tag{45}$$

where $a = \sqrt{2K}$.

To derive Eq. (45), we calculate the integration term $\int_{-a}^{a}\lambda^2 h_i^2(\lambda)\,\mathrm{d}\lambda$. We substitute the normalized Hermite polynomials into the probabilists' Hermite polynomials, which has the relationship $h_i(\lambda) = (\sqrt{\pi}i!)^{-\frac{1}{2}} e^{-\frac{\lambda^2}{2}} H_i\left(\sqrt{2}\lambda\right)$. Then, the integration term can be calculated as:

$$\begin{aligned}&\int_{-a}^{a}\lambda^2 h_i^2(\lambda)\,\mathrm{d}\lambda = \frac{1}{\sqrt{\pi}i!}\int_{-a}^{a}\lambda^2 e^{-\lambda^2}H_i^2\left(\sqrt{2}\lambda\right)\mathrm{d}\lambda \\ &= \frac{1}{\sqrt{2\pi}i!}\int_{-\sqrt{2}a}^{\sqrt{2}a}\frac{y^2}{2}e^{-\frac{y^2}{2}}H_i^2(y)\,\mathrm{d}y \left(\text{by setting } y = \sqrt{2}\lambda\right) \\ &= \frac{1}{\sqrt{2\pi}i!}\int_{-\sqrt{2}a}^{\sqrt{2}a}\frac{y^2}{2}H_i(y)(-1)^i\frac{\mathrm{d}^i}{\mathrm{d}y^i}e^{-\frac{y^2}{2}}\mathrm{d}y \\ &\left(\text{Since } H_i(y) = (-1)^i e^{\frac{y^2}{2}}\frac{\mathrm{d}^i}{\mathrm{d}y^i}e^{-\frac{y^2}{2}}\right) \\ &\overset{[38]}{=} \frac{1}{\sqrt{2\pi}}\int_{-\sqrt{2}a}^{\sqrt{2}a}\frac{y^2}{2}e^{-\frac{y^2}{2}}\mathrm{d}y = \frac{1}{2} - \frac{ae^{-a^2}}{\sqrt{\pi}} - \Phi\left(-\sqrt{2}a\right),\end{aligned} \tag{46}$$

where $\Phi(x)$ is the CDF of the standard normal distribution. If the solution of the integration term is denoted as $I(a)$, the variance σ_0^2 is $\sigma_0^2 = \frac{2K-1}{2K}I\left(\sqrt{2K}\right)$.

In order to obtain the detection threshold with a given false alarm rate and the detection probability, the null and alternative distributions of the detection statistic Z_R should be first derived.

Under the hypothesis $\mathcal{H}_1$, $Z_R|\mathcal{H}_1$ is also a normal distribution with mean $\mu_1 = \alpha\sum_{h=1}^{K}\mathrm{E}\left[\widetilde{\Phi}_{\mathbf{S}}(h,h)\right]$ and variance $\sigma_1^2 = \alpha^2\sum_{h=1}^{K}\mathrm{Var}\left[\widetilde{\Phi}_{\mathbf{S}}(h,h)\right]$, related to the power of the transmitted signal and the variance of noise. The PDFs of $Z_R|\mathcal{H}_0$ and $Z_R|\mathcal{H}_1$ are:

$$f(Z_R|\mathcal{H}_0) = \frac{1}{\sqrt{2\pi}\sigma}e^{-\frac{Z_R^2}{2\sigma^2}}, \tag{47}$$

and

$$f(Z_R|\mathcal{H}_1) = \frac{1}{\sqrt{2\pi}\sigma_1}e^{-\frac{(Z_R-\mu_1)^2}{2\sigma_1^2}}. \tag{48}$$

Therefore, whether or not the target exists can be determined by the detection threshold ξ_{Eigen}, that is:

$$Z_R\begin{cases}\geq \xi_{Eigen}, & \mathcal{H}_1 \\ < \xi_{Eigen}, & \mathcal{H}_0\end{cases}, \tag{49}$$

where the threshold ξ_{Eigen} can be obtained with a given false alarm rate P_{fa}^2,

$$\xi_{Eigen} = \sqrt{2}\sigma\mathrm{erf}^{-1}\left(1-2P_{fa}^2\right), \tag{50}$$

where $\mathrm{erf}^{-1}(x)$ is the inverse function of error function $\mathrm{erf}(x)$.

The detection probability with the threshold ξ_{Eigen} is determined by:

$$P_D = \int_{\xi_{Eigen}}^{+\infty} f(Z_R|\mathcal{H}_1)\,\mathrm{d}Z_R = \frac{1}{2}\left[1 - \mathrm{erf}\left(\frac{\xi_{Eigen}-\mu_1}{\sqrt{2}\sigma_1}\right)\right]. \tag{51}$$

B. Implementation of the Proposed Method

The diagram of the proposed method is shown in Fig. 3. There are three main parts in the scheme: (1) Acquisition of data, (2) statistics for identification of ultra-high speed targets, and (3) detection of ultra-high speed targets and determination of the target number and location.

Part (1): Acquisition of data.

Suppose the required detection range is from r_0 to r_1, which satisfies the condition that $r_1 - r_0$ is an integral multiple $L = \frac{r_1-r_0}{\Delta r}$ of the radar range resolution $\Delta r = \frac{C}{2B}$, where C is the light velocity. At an azimuth and pitching angle, the radar receiver can obtain a string of the samples, whose sampling interval in the distance domain is equal to the range resolution during a short observation time T_O. After demodulation and PC have been applied to the samples in each PRI T_I, a two-dimensional matrix R in the range and slow-time domain can be formulated. Suppose the velocity of the target which we need to detect is V. Then, the number of the detection range resolution is $K = \lceil\frac{VT_O}{\Delta r}\rceil$, where $\lceil\cdot\rceil$ denotes the ceiling function. The detection matrix can be defined as $R_{M\times K}^l =$

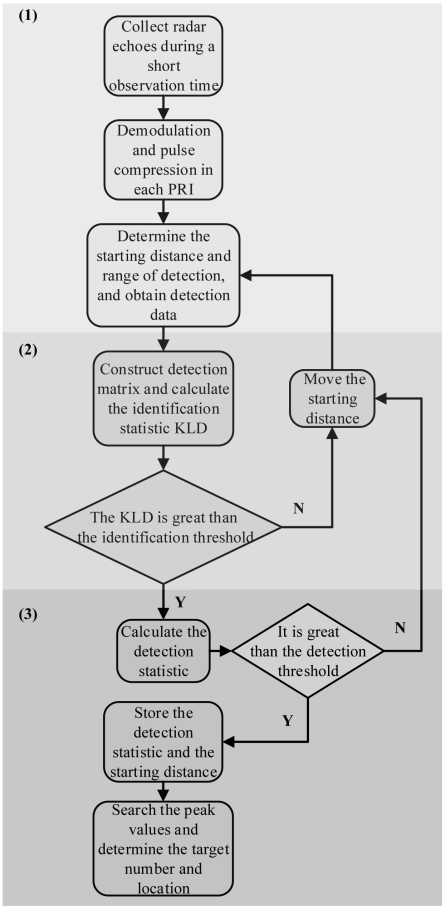

Fig. 3. Flowchart of the proposed method.

$r(i,j), i = 1, 2, \cdots, M, j = l+1, l+2, \cdots, l+K$, where $M = \lfloor \frac{T_O}{T_I} \rfloor$, $\lfloor \cdot \rfloor$ denotes the floor function, and l is an indicator of the starting detection distance with $l = 0, 1, \cdots, L-1$.

Part (2): Statistics for identification of ultra-high speed targets.

For generating the statistics, the indicator l starts from 0, and the identification statistics D_{KL}^{l} can be formed as shown in Fig.2. $R_{M\times K}^{l}$ is the input and D_{KL}^{l} is the output. Suppose we now detect the ultra-high speed targets from the low speed targets whose velocity is less than V_0. The parameter P can be obtained as $P = \lceil \frac{V_0 T_O}{\Delta r} \rceil$, and the identification threshold β_I can be determined by Eq. (40) with the given false alarm rate P_{fa}^{1} and corresponding false identification rates $P_{fi}^{v_{th}}$ calculated by Eq. (42). If the identification statistics D_{KL}^{l} is less than the identification threshold β_I, we know that there is no ultra-high speed target in the detection area under the false alarm rate P_{fa}^{1} and false identification rates $P_{fi}^{v_{th}}$, or the ultra-high speed target which exists in the detection area cannot be effectively detected. We then continue to investigate the identification statistics $D_{KL}^{l'}$ for the next detection area, i.e. $l' = l+1$. However, if the identification statistics D_{KL}^{l} is equal to or greater than the identification threshold β_I, there is an ultra-high speed target in the detection area with the false alarm rate P_{fa}^{1} and false identification rates $P_{fi}^{v_{th}}$. We apply the detection matrix to the eigenvalues based detector for further evaluation of whether or not an ultra-high speed target exists.

Part (3): Detection of ultra-high speed targets and determination of the target number and location.

After having evaluated the detection matrix $R_{M\times K}^{l}$ with the false identification rates $P_{fi}^{v_{th}}$ and the false alarm rate P_{fa}^{1}, we now check this matrix with the eigenvalue based detector for the final decision of whether or not an ultra-high speed target exists in the detection area. According to Eq. (44), the detection statistics Z_R^l can be derived by:

$$Z_R^l = \alpha \sum_{h=1}^{K} \widetilde{\lambda}_h^l, \tag{52}$$

where $\widetilde{\lambda}_h^l, h = 1, 2, \cdots, K$ are the eigenvalues of $\widetilde{\Phi}_R$ which come from the detection matrix $R_{M\times K}^{l}$.

If the detection statistics Z_R^l is less than the detection threshold ξ_{Eigen}, there is no ultra-high speed target in the detection area with the false alarm rate P_{fa}^{2}. Otherwise, there is an ultra-high speed target in the detection area. We store the detection statistics Z_R^l in an empty-vector $\Theta_{1\times L}$, and the stored element is $\Theta(l+1) = Z_R^l$. When the search of the indicator l is completed, the empty elements of vector $\Theta_{1\times L}$ are replaced by zero. We then look for the peaks of vector $\Theta_{1\times L}$, that is:

$$[\mathbf{A}_{pk}, \mathbf{Q}_{loc}] = findpeaks\left(\Theta_{1\times L}\right), \tag{53}$$

where the elements of vector $\mathbf{A}_{pk}$ refer to the peak values, and the elements of vector $\mathbf{Q}_{loc}$ are the corresponding indicators for us to render the detection distance.

We initiate the starting distance of detection as the starting distance of the ultra-high speed target, which enables us to obtain better detection statistics. The length of vector $\mathbf{A}_{pk}$ refers to the number of ultra-high speed targets, and the starting distance of ultra-high speed targets is $r_0 + (\mathbf{Q}_{loc} - \mathbf{I})\Delta r$, where the elements of vector $\mathbf{I}$ are set to be one, having the same length as that of vector $\mathbf{Q}_{loc}$.

C. Computational Complexity Analysis

The computational complexity of the proposed identification and detection method for ultra high speed targets mainly comes from the calculation of covariance matrix $\Phi_{\mathbf{R}}$ shown in Eq. (15) and the eigenvalue decomposition of matrix $\Phi_{\mathbf{R}}$. Suppose the detection range contains L range bins, and the size of the test matrix $\mathbf{R}$ is $M \times K$. The computational complexity of the sample covariance matrix is $\mathcal{O}\left(K^2 M\right)$. For the eigenvalue decomposition of matrix $\Phi_{\mathbf{R}}$, the computational complexity is $\mathcal{O}\left(K^3\right)$. Since we need to search over L range bins, the computational complexity of the proposed method can be written as:

$$\mathcal{O}\left(K^2 ML + K^3 L\right). \tag{54}$$

Since $M > K$, the computational complexity of the proposed method can be simplified as $\mathcal{O}\left(K^2 ML\right)$.

Now, we compare our proposed method with the existing RFrFT and RLVD methods, which are recognised maneuvering target detection and estimation methods. The FrFT is the

core component of the RFrFT method, whose computational complexity is $\mathcal{O}\left(p_1 M \log_2 M\right)$, where, p_1 is the number of the searching transform angles in the FrFT. In addition, the RFrFT method also needs to search for the motion parameters, such as range, initial velocity and acceleration, where the searching number can be denoted as L, p_2 and p_3 respectively. Thus, the total computational complexity of the RFrFT method is $\mathcal{O}\left(p_1 p_2 p_3 M L \log_2 M\right)$. To successfully explore the motion parameters, the searching numbers p_1, p_2, p_3 must be large enough, while the value of parameter K is very small (usually $K \leq 30$) in our method. Besides, the echos of ultra high speed targets accompany Doppler ambiguity, and the RFrFt method requires extra computation complexity to deal with the problem. Therefore, the computational complexity $\mathcal{O}\left(K^2 M L\right)$ of our method is much less than that of the RFrFT method.

Since the computational complexity of LVD based on 2D FFT is $\mathcal{O}\left(M^2 \log_2 M\right)$ [19] and the RLVD method also needs to search for the motion parameters, such as range, initial velocity and acceleration, wherein the searching numbers are denoted as L, $p2$ and $p3$ respectively. Therefore, the total computational complexity of the RLVD method is

$$\mathcal{O}\left(Lp2p3M^2 \log_2 M\right), \tag{55}$$

where, the searching numbers $p2$ and $p3$ must be large enough to find the true motion parameters. Obviously, the computational complexity $\mathcal{O}\left(K^2 M L\right)$ of our proposed method is also much less than that of the RLVD method.

VI. Simulation Results

In this section, we first validate the correctness of the proposed method in theory by comparing the expected values (marked as Theo) using the derived equations against the experimental values (marked as Monte) via the standard Monte Carlo method [40]. Then, the identification and detection performance are simulated to verify the superiority of our proposed method. Finally, the system performance of the proposed method is demonstrated by applying it to a simulated detection scenario. In the simulations, the transmitted signal is a narrow-band LFM signal, where the parameters are empirically set as: Pulse repetition time $T_I = 0.001s$, emitter wavelength $\lambda = 0.1m$, waveform bandwidth $B = 3.75MHz$, and pulse duration $T_P = 2.7us$. For demonstration purposes, we suppose that the target flies away from the radar and the angle between the target velocity and the line of sight to the radar is zero.

A. Validation of the Theoretical Analysis

In this subsection, the correctness of the distributions of the identification and detection statistics, formulated as Eqs. (33), (39), (47) and (48), are verified.

1) The Distribution of Identification Statistics: The correctness of the distributions of identification statistics D_{KL}, formulated as Eqs. (33) and (39), can justify the distribution of the eigenvalues of matrix $\widetilde{\Phi}_{\mathbf{R}}$ shown in Eq. (26). It also verifies the correctness of the identification threshold by Eq. (40), identification probabilities by Eq. (41), and the false identification rate by Eq. (42).

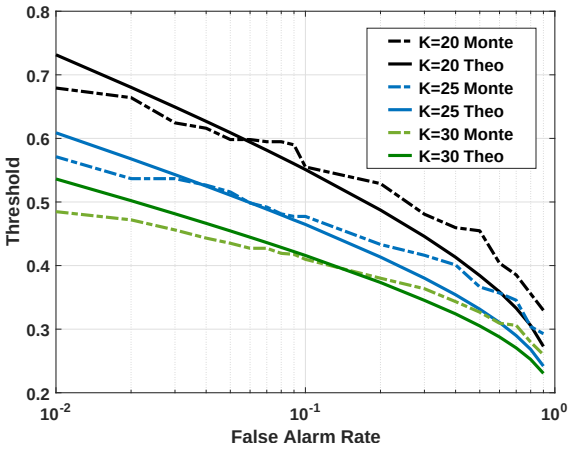

Fig. 4. Thresholds versus false alarm rates for the identification stage with different K test range bins, where the dotted lines denote the experimental values and the solid lines denote the expected values by Eq. (40) ($T_O = 0.1s$).

For validating the correctness of the identification statistics in the case where the target does not exist, we suppose the observation time T_O is $0.1s$, suggesting that the row number M of the test matrix is set to be 100, leading to the verification results shown in Fig. 4 with K test range bins. It clearly demonstrates that our derived Gamma distribution of the identification statistics, formulated in Eq. (33), is correct as the thresholds by Eq. (40) (shown as solid lines) are very close to those of the Monte Carlo simulations (shown as dotted lines) for different false alarm rates.

For validating the correctness of the distributions of the identification statistics in the case where a target exists, we assume that the velocity of the ultra high speed target is $20Ma$, the acceleration is $10m/s^2$, the observation time T_O is $0.1s$, and the target starts moving at the beginning of the observation time. Using the identification velocity, we can determine the number K of the test range bins is 20. Fig. 5 denotes the comparisons between the expected values (shown as red lines) by Eq.(41) and the experimental values (shown as blue lines) by the Monte Carlo method with four SNRs ($-5dB$, $-3dB$, $3dB$ and $5dB$). As shown in Fig. 5, for each SNR, we see that the curve of the experimental values looks similar to that of the theoretical values, from which we conclude that the derived distribution with the CDF formulated as Eq. (39) is correct. From the four subfigures, we observe that the higher the SNR is, the more the identification statistics D_{KL} is, reflected by the parameter $C\left(v, \Phi_{\mathbf{S}}\right)$ of the derived distribution. It suggests that the higher the SNR of the echoes is, the better identification performance can be achieved.

2) Distribution of Detection Statistics: The validation of the correctness of the distributions of the detection statistics Z_R, formulated as Eqs. (47) and (48), can not only verify the correctness of the means μ_0, μ_1, and the variances σ_0, σ_1, but also verify the correctness of the detection thresholds ξ_{Eigen} by Eq. (50), and the detection probabilities by Eq. (51).

For the validation of detection statistics $Z_R|\mathcal{H}_0$, we suppose the observation time T_O is $0.1s$, and the verification results are shown in Fig. 6 with K test range bins. In Fig. 6, we notice

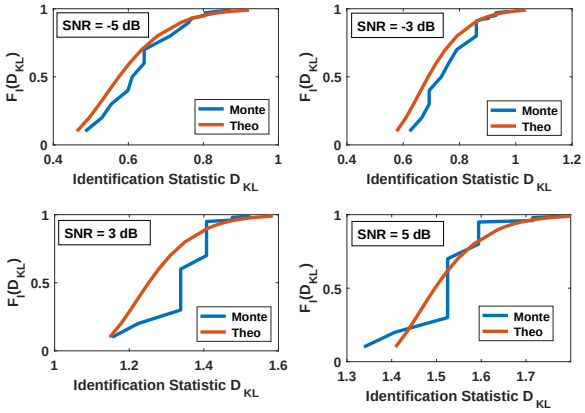

Fig. 5. Validation of the cumulative distribution of the identification statistics in the case where the target exists with different SNRs: Blue lines denote the experimental results and red lines denote the expected values by Eq. (41).

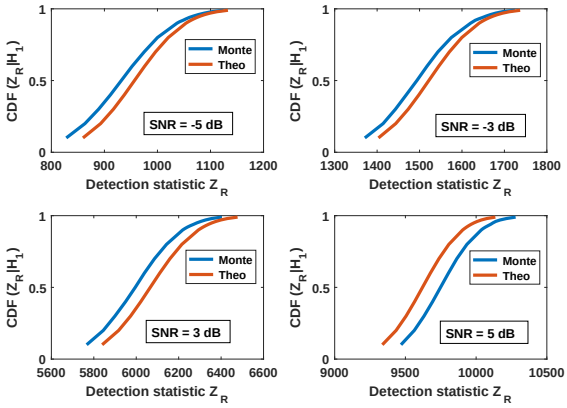

Fig. 7. Validation of the cumulative distribution of identification statistics $Z_R|\mathcal{H}_1$ with different SNRs, where blue lines denote the experimental values and the red lines denote the theoretical values by Eq. (51).

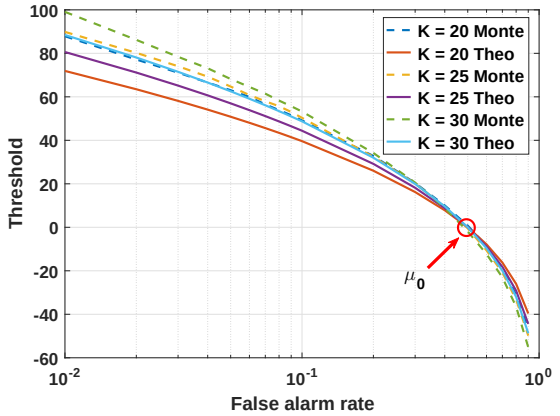

Fig. 6. Thresholds versus false alarm rates for the detection stage with different K test range bins, where dotted lines denote the experiment values and the solid lines denote the theoretical values using Eq. (50).

that the detection threshold curve by the Monte Carlo method looks similar to that of Eq. (50) except for some rotations. Meanwhile, we also observe that the detection thresholds of the Monte Carlo method, the estimation of mean μ_0, are close to zero when the false alarm rate is 0.5, and the rotation angles of these curves, representing the estimation errors of variance σ^2, are small. Thus, we conclude that the distribution of the detection statistics in the case where the target does not exist approaches to a normal distribution, shown as Eq. (47).

For the validation of detection statistics $Z_R|\mathcal{H}_1$, we also assume that the velocity of the ultra high speed target is $20Ma$, the acceleration is $10m/s^2$, the observation time T_O is $0.1s$, and the target starts moving at the beginning of the observation time. Supposing the identification velocity is $20Ma$, we can determine the number K of the test range bins as 20. The comparison between the theoretical values (shown as red lines) by Eq. (51) and the experimental values (shown as blue lines) by the Monte Carlo method is achieved with four different SNRs ($-5dB$, $-3dB$, $3dB$ and $5dB$). As shown in Fig. 7, for each SNR, we find that the curve of the experimental values looks similar to that of the theoretical values. The discrepancy between these curves attributes to the estimation error of mean μ_1 and variance σ_1^2 shown in Eq. (48) for the Monte Carlo method. We believe that the derived distribution whose PDF is formulated as Eq. (48) is correct. From the four subfigures, we observe that the higher the SNR is, the better the detection statistics $Z_R|\mathcal{H}_1$ become, reflected by the mean μ_1 of the derived distribution. This indicates that the higher the SNR of the echoes, the better the detection performance for ultra high speed targets is, given a proper false alarm rate.

B. Identification Performance Analysis

Although the established identification methods have shown promising performance, they have to seek appropriate motion parameters in a large search space. In real battle fields, it is extremely demanding to efficiently and accurately estimate the velocity of an ultra high speed target. Here, we compare our identification method against the standard Doppler method, which is reliable and efficient, instead of other intelligent but time-consuming detection methods to evaluate the identification performance of our proposed method.

The simulated observation time T_O is $0.15s$, and the number K of the test range bins is 20. Suppose the target starts moving at the beginning of the observation time. In order to study the identification performance at different identification velocities, the identification probabilities of each velocity are simulated with the false alarm rate $P_{fa}^1 = 10^{-3}$ in different simulated SNRs, which are listed in Table I (for the identification of high-hypersonic target with velocity $15Ma$), Table II (for the identification of a hypersonic target with velocity $8Ma$) and Table III (for the identification of a high speed target with velocity $4Ma$). In each table, we notice that, for the identified velocity, its identification performance is the best, while, for other velocities, the further a velocity is away from the identified velocity, the worse the identification performance is. However, the Doppler method always has a superior identification performance for low speed targets, but has poor identification performance for ultra high speed targets. This is because the higher the velocity of the target is, the less the energy is accumulated in one range bin for the established identification

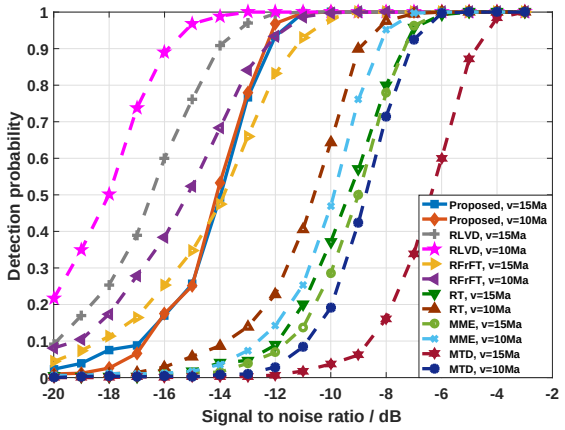

Fig. 8. Detection probability vs signal to noise ratio for high-hypersonic targets with velocities 10Ma and 15Ma ($B = 3.75MHz$).

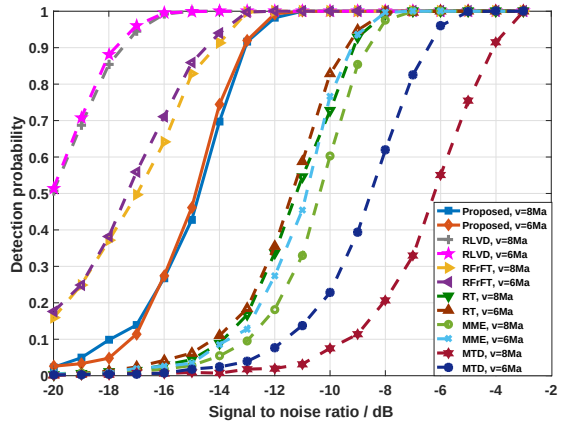

Fig. 9. Detection probability vs signal to noise ratio for hypersonic targets with velocities 6Ma and 8Ma ($B = 7.5MHz$).

methods with low computational complexity. Therefore, our proposed identification method supports identification if the target velocity from the other velocities. For the identification velocity in each table, our identification performance is obviously superior to the Doppler method. For example, in Table I, the identification probabilities of the identified velocity $15Ma$ are all 100%, while those of the Doppler method are all 0, with the simulated SNRs. Therefore, our proposed identification method has much better identification performance than the standard identification methods which have low computational complexity. Furthermore, from Tables I, II and III, our proposed method is suitable for high speed, hypersonic and high-hypersonic targets, respectively.

C. Detection Performance Analysis

To demonstrate the detection performance of our proposed method, we compare our method against three state of the art detection methods, including RLVD, RFrFT, maximum-minimum eigenvalue (MME) [41], [42], MTD and RT. They are the most advanced methods recently developed in the field. The RLVD and RFrFT methods are advanced coherent integration methods with high computational complexity. MTD is a classical coherent integration method with light computational complexity. MME is an advanced spectrum sensing method based on the eigenvalues of the received signals. RT is an incoherent integration method. Simulation parameters are set to be: the observation time T_O is $0.15s$, the number K of test range bins is 20, and the false alarm rate P_{fa}^2 is 10^{-3}. We also assume that the target starts moving at the beginning of the observation time. We conduct simulations for high-hypersonic targets with velocities $10Ma$, $15Ma$ and the hypersonic targets with velocities $6Ma$, $8Ma$. For high-hypersonic targets, the bandwidth of the transmitted signal is $3.75MHz$. For hypersonic targets, the bandwidth of the transmitted signal is $7.5MHz$. The acceleration is set as $10m/s^2$.

Figs. 8 and 9 show the detection probability curves with different SNRs for high-hypersonic and hypersonic targets, respectively. As shown in Fig. 9, even for the detection of a target with a high speed $6Ma$, the detection performance of RFrFT is still better than that of our proposed detection method. The RFrFT method can detect the target of velocity $6Ma$ effectively with the SNRs of $-13dB$ and above, while our proposed method needs to be with the SNRs of $-11dB$ to implement an effective detection. With the increase of the target velocity, the detection performance of RFrFT continues to decline, while the performance of our proposed method for ultra-high speed targets almost remains unchanged. As shown in Fig. 8, when the velocity of the moving target is $10Ma$, the RFrFT method has almost the same detection performance as our proposed detection method, both of which can detect the target effectively until the signal-to-noise ratio (SNR) declines to $-11dB$. Furthermore, when the velocity of the moving target increases to $15Ma$, the SNR of an effective detection needs more than $-10dB$ for the RFrFT method, whilst the SNR of our proposed detection method still stay around $-11dB$. As shown in Figs. 8 and 9, although the RLVD method is still based on the assumption that the Doppler frequency is LFM, the degenerative detection performance of RLVD is better than that of the RFrFT method and our proposed detection method for ultra-high speed targets. However, with the increase of the target velocity, the degradation of the detection performance of the RLVD method continues, while our proposed coherent-like detection method can almost keep its performance. According to the analysis of computational complexity presented in Section V-C, our proposed method has lower computational complexity than the RFrFT method and the RLVD method. Thus, our proposed method is efficient for the short time detection. In addition, for different velocities, our proposed method maintains consistent detection performance, while all the other methods have unstable detection performance. Therefore, our proposed detection method is robust against different noise levels. From Figs. 8 and 9, we also observe that the lower the velocity, the higher the detection performance achieved by each detection method.

D. Identification and Detection of Moving Targets

In the previous subsections, we have validated the superiority of our proposed method in the identification and detection

TABLE I
IDENTIFICATION PROBABILITIES OF TARGETS WITH DIFFERENT VELOCITIES IN DIFFERENT SIGNAL TO NOISE RATIOS (SNRS) FOR THE IDENTIFICATION OF HIGH-HYPERSONIC TARGET WITH VELOCITY $15Ma$ ($P_{fa}^1 = 10^{-3}$, $B = 3.75MHz$, $K = 20$, $T_O = 0.15s$).

Velocity	Method	SNR											
		$-2dB$	$-1dB$	$0dB$	$1dB$	$2dB$	$3dB$	$4dB$	$5dB$	$6dB$	$7dB$	$8dB$	$9dB$
4 Ma	**Proposed method**	**0.097**	**0.105**	**0.096**	**0.101**	**0.119**	**0.144**	**0.143**	**0.133**	**0.142**	**0.134**	**0.138**	**0.149**
	Doppler method	0.080	0.192	0.327	0.514	0.737	0.857	0.913	0.926	0.975	0.980	0.986	0.998
6 Ma	**Proposed method**	**0.161**	**0.212**	**0.222**	**0.210**	**0.244**	**0.269**	**0.257**	**0.284**	**0.254**	**0.248**	**0.255**	**0.264**
	Doppler method	0.008	0.011	0.023	0.083	0.186	0.331	0.561	0.731	0.858	0.890	0.928	0.957
8 Ma	**Proposed method**	**0.296**	**0.365**	**0.442**	**0.594**	**0.683**	**0.720**	**0.720**	**0.759**	**0.763**	**0.760**	**0.733**	**0.735**
	Doppler method	0	0.001	0.007	0.007	0.03	0.056	0.124	0.238	0.429	0.551	0.670	0.737
10 Ma	**Proposed method**	**0.498**	**0.583**	**0.763**	**0.892**	**0.904**	**0.958**	**0.998**	**1**	**1**	**1**	**1**	**1**
	Doppler method	0	0	0	0	0	0	0	0.002	0.005	0.004	0.020	0.054
15 Ma	**Proposed method**	**1**	**1**	**1**	**1**	**1**	**1**	**1**	**1**	**1**	**1**	**1**	**1**
	Doppler method	0	0	0	0	0	0	0	0	0	0	0	0

TABLE II
IDENTIFICATION PROBABILITIES OF TARGETS WITH DIFFERENT VELOCITIES IN DIFFERENT SIGNAL TO NOISE RATIOS (SNRS) FOR THE IDENTIFICATION OF HYPERSONIC TARGET WITH VELOCITY $8Ma$ ($P_{fa}^1 = 10^{-3}$, $B = 7.5MHz$, $K = 20$, $T_O = 0.15s$).

Velocity	Method	SNR											
		$-2dB$	$-1dB$	$0dB$	$1dB$	$2dB$	$3dB$	$4dB$	$5dB$	$6dB$	$7dB$	$8dB$	$9dB$
4 Ma	**Proposed method**	**0.341**	**0.401**	**0.503**	**0.604**	**0.703**	**0.706**	**0.724**	**0.699**	**0.704**	**0.725**	**0.738**	**0.763**
	Doppler method	0.162	0.378	0.583	0.732	0.829	0.927	1	1	1	1	1	1
6 Ma	**Proposed method**	**0.914**	**0.993**	**1**	**1**	**1**	**1**	**1**	**1**	**1**	**1**	**1**	**1**
	Doppler method	0.003	0.003	0.018	0.062	0.083	0.181	0.331	0.598	0.832	0.961	1	1
8 Ma	**Proposed method**	**1**	**1**	**1**	**1**	**1**	**1**	**1**	**1**	**1**	**1**	**1**	**1**
	Doppler method	0	0	0.003	0.002	0.008	0.036	0.047	0.132	0.254	0.468	0.690	0.923
10 Ma	**Proposed method**	**0.457**	**0.915**	**1**	**1**	**1**	**1**	**1**	**1**	**1**	**1**	**1**	**1**
	Doppler method	0	0	0	0	0.003	0.005	0.011	0.028	0.080	0.170	0.329	0.564
15 Ma	**Proposed method**	**0.062**	**0.111**	**0.480**	**0.952**	**1**	**1**	**1**	**1**	**1**	**1**	**1**	**1**
	Doppler method	0	0	0	0	0	0	0	0	0	0.008	0.020	0.042

TABLE III
IDENTIFICATION PROBABILITIES OF TARGETS WITH DIFFERENT VELOCITIES IN DIFFERENT SIGNAL TO NOISE RATIOS (SNRS) FOR THE IDENTIFICATION OF HIGH SPEED TARGET WITH VELOCITY $4Ma$ ($P_{fa}^1 = 10^{-3}$, $B = 15MHz$, $K = 20$, $T_O = 0.15s$).

Velocity	Method	SNR											
		$-2dB$	$-1dB$	$0dB$	$1dB$	$2dB$	$3dB$	$4dB$	$5dB$	$6dB$	$7dB$	$8dB$	$9dB$
4 Ma	**Proposed method**	**1**	**1**	**1**	**1**	**1**	**1**	**1**	**1**	**1**	**1**	**1**	**1**
	Doppler method	0.009	0.025	0.049	0.139	0.241	0.459	0.738	0.903	0.980	0.998	1	1
6 Ma	**Proposed method**	**0.194**	**0.663**	**0.996**	**1**	**1**	**1**	**1**	**1**	**1**	**1**	**1**	**1**
	Doppler method	0	0	0.002	0.005	0.011	0.037	0.088	0.168	0.328	0.555	0.762	0.932
8 Ma	**Proposed method**	**0.040**	**0.119**	**0.510**	**0.937**	**1**	**1**	**1**	**1**	**1**	**1**	**1**	**1**
	Doppler method	0	0	0	0	0	0.005	0.018	0.033	0.082	0.157	0.294	0.569
10 Ma	**Proposed method**	**0.020**	**0.058**	**0.127**	**0.490**	**0.958**	**1**	**1**	**1**	**1**	**1**	**1**	**1**
	Doppler method	0	0	0	0.002	0.002	0	0.003	0.002	0.008	0.027	0.063	0.143
15 Ma	**Proposed method**	**0.013**	**0.016**	**0.023**	**0.063**	**0.178**	**0.600**	**0.983**	**1**	**1**	**1**	**1**	**1**
	Doppler method	0	0	0	0	0	0	0	0	0	0	0.001	0.004

stages. In this subsection, we will apply the proposed method to two real battle scenes: in scene 1, there are four targets: two high speed targets ($v = 2$Ma, $r_0 = 200Km$ and $v = 4$Ma, $r_0 = 202.5Km$) and two ultra high speed targets ($v = 10$Ma, $r_0 = 201.3Km$ and $v = 15$Ma, $r_0 = 203.7Km$); in scene 2, there are also four targets: two high speed targets ($v = 2$Ma, $r_0 = 200Km$ and $v = 4$Ma, $r_0 = 200.7Km$) and two ultra high speed targets ($v = 8$Ma, $r_0 = 200.3Km$ and $v = 10$Ma, $r_0 = 201.1Km$). The acceleration of all the targets is $10m/s^2$. The simulated SNR is $0dB$. The bandwidths of the transmitted signal in the two scenes are $3.75MHz$ and $15MHz$ respectively. The received signals in the range and slow-time domains, after the matched filtering, are shown in Figs. 10 and 13, respectively. The left subfigure of Fig. 11 shows the range-Doppler of the radar echoes. We can hardly observe these targets in the frequency domain. The target energy is distributed over different range bins and Doppler cells for each target. From Fig. 10 and the left subfigure of Fig. 11, we observe that although the observation time ($0.117s$) is very short, there are still severe ARU and DFM effects to influence the detection.

The right subfigure of Fig. 11 shows the detection result of the traditional MTD method. Since the MTD method cannot solve the ARU and DFM problems, the target energy is still distributed over different range bins after the MTD processing, which requires the SNR to be further improved. In addition, since the ARU and DFM effects of the ultra high speed target are more serious than those of the high speed target, the outputs of the ultra high speed targets are mixed with the output of the low speed targets for the MTD method as

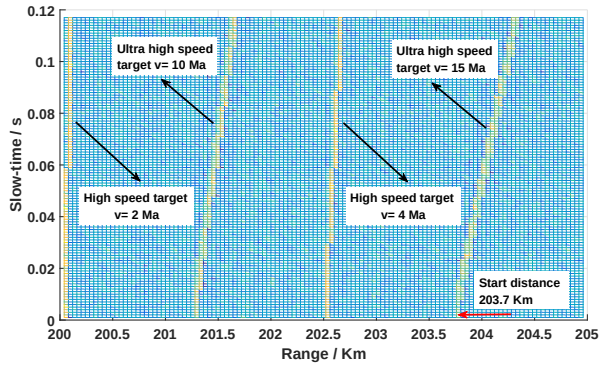

Fig. 10. Radar echoes of four targets in the range and slow-time domain, two of which are high speed targets (2 Ma, 4 Ma) and two high-hypersonic targets (10 Ma, 25 Ma), after the matched filtering, under the Gaussian noise background ($SNR = 0dB$, $B = 3.75MHz$, $T_O = 0.117s$).

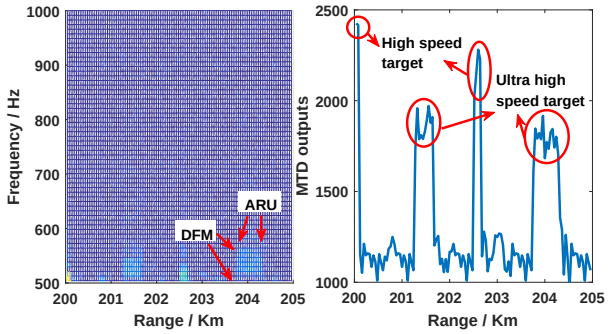

Fig. 11. Target detection using the MTD method: The left subfigure is the range-Doppler analysis of the radar's returns. The right subfigure is the MTD's outputs in each range bin ($T_O = 0.117s$).

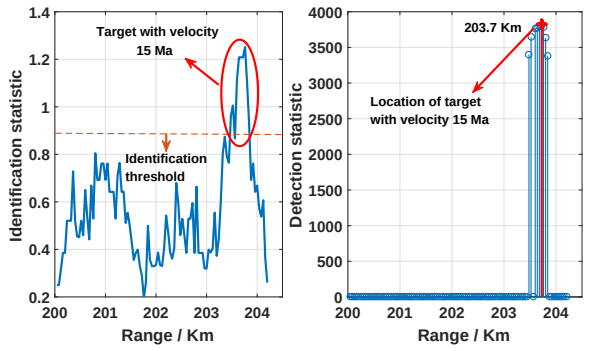

Fig. 12. Identification and detection of an ultra high speed target with velocity $15Ma$: The left subfigure is the output of the identification. The right subfigure is the output of the detection ($T_O = 0.117s$, $P_{fa}^1 = 10^{-3}$).

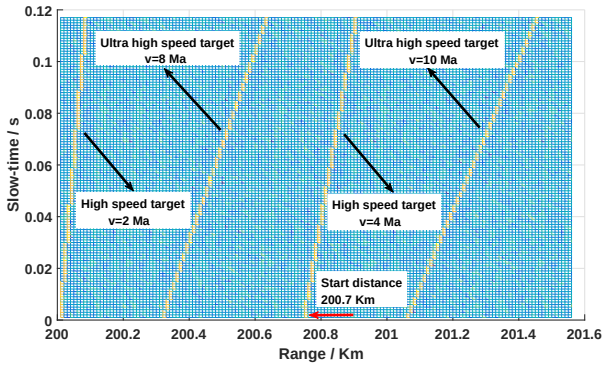

Fig. 13. Radar echoes of four targets in the range and slow-time domain, two of which are high speed targets (2 Ma, 4 Ma) and two hypersonic targets (8 Ma, 10 Ma), after the matched filtering, under the Gaussian noise background ($SNR = 0dB$, $B = 15MHz$, $T_O = 0.117s$).

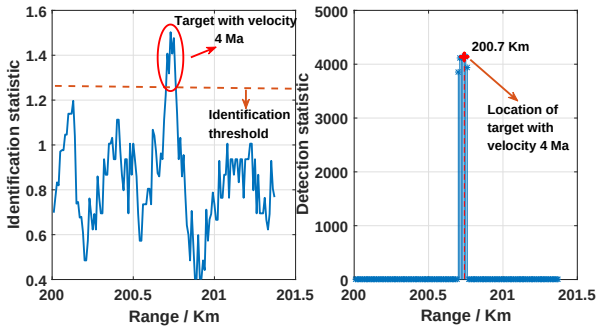

Fig. 14. Identification and detection of a high speed target with velocity $4Ma$: The left subfigure is the output of the identification. The right subfigure is the output of the detection statistics ($T_O = 0.117s$, $P_{fa}^1 = 10^{-6}$).

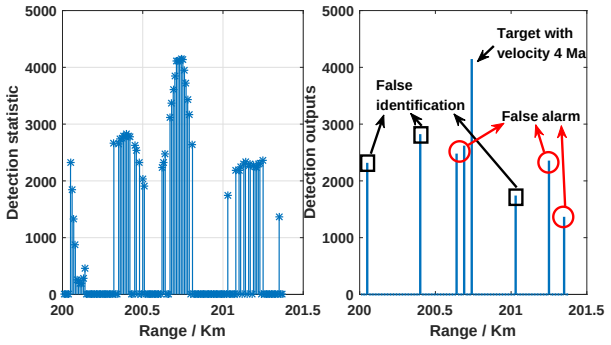

Fig. 15. Identification and detection of a high speed target with velocity $4Ma$: The left subfigure is the output of the detection statistics. The right subfigure is the output of the detection ($T_O = 0.117s$, $P_{fa}^1 = 10^{-3}$).

shown in the right subfigure of Fig. 11. Thus, we are unable to identify the ultra high speed targets from the high speed targets by using the traditional MTD method.

However, the identification output for the identified velocity $15Ma$ is larger than those of the other velocities using our proposed method, as shown in the left subfigure of Fig. 12. Therefore, we can successfully identify the target with velocity $15Ma$ using the identification method with false alarm rate 10^{-3}, whose value is 0.889 (the red dotted line shown in the figure). We can reuse the test matrix data with the identification statistics exceeding the identification threshold and their starting distance for the next detection stage. The right subfigure of Fig. 12 reports the detection results of the ultra high speed target whose velocity is 15Ma. After having computed the detection statistics of those test matrix data, we can retrieve the number and location of the ultra high speed target searching for the maximum from the values of the detection statistics over the detection threshold. As the right subfigure of Fig. 12 shows, there is only one ultra high

speed target with velocity 15Ma and its starting distance is $203.7Km$, which is the same as shown in the battle scene Fig. 10.

Fig. 14 reveals the identification and detection results of a high speed target with velocity $4Ma$. Comparing the identification threshold with false alarm rate 10^{-6}, whose value is 1.251 (red dotted line shown in the left subfigure of Fig. 14), we obtain the correct number and location of the high speed target whose velocity is $4Ma$. Therefore, our proposed identification and detection method can be applied to both high and ultra-high speed targets. Also, like other detection methods, if we set up correct thresholds and pick up the identification threshold with a larger false alarm rate, such as 10^{-3}, we will detect more false targets and true targets whose velocities are not correct, as shown in the right subfigure of Fig. 15.

VII. Conclusion

The existing advanced target coherent detection methods normally require high computational complexity, which is unacceptable for detecting ultra high speed targets in a short observation time. Even though these existing detection methods without knowing motion parameters have low computational complexity, they often lack sufficient ability to identify different velocities. In this paper, a coherent-like detection method along with velocity identification without the need to search the motion parameter space has been proposed by balancing the performance of identification, detection and computational complexity. Since the proposed method does not use the phase information of the echoes, it is not a standard coherent integration method. Our proposed method was based on the assumption that the expectation of the eigenvalues of Wigner matrices is equal to zero, namely the eigenvalue cancellation of background noise, to improve the SNR of the detection system. The drawback of pursuing high detection performance is that the detection method loses the information about the differences of eigenvalues between different velocities, and therefore it cannot identify different velocities effectively. Therefore, we intend to design an identification method for different velocities. The distribution and mean function of the eigenvalues of an additive Wigner matrix was utilized to identify the target velocity while detecting ultra high speed targets. The proposed method can detect the interesting target well by filtering the targets with less interesting velocities in a general short-time detection scenario that there are no overlapping range bins between the targets. In this paper, the distributions of the identification and detection statistics with or without a target have been derived in a solid form and justified in the simulations. The superiority and operability of our proposed method were also validated.

Acknowledgement

The authors would like to thank the anonymous reviewers and the editor for their constructive comments and suggestions to the paper.

References

[1] R. A. Dietrick, "Hypersonic flight: time to go operational," *Technical Report*, Defense Technical Information Center, Feb. 2013.
[2] C. Brink, "X-51A flight test status update," in *Proc. IEEE 43rd Annual International Symposium of the Society of Flight Test Engineers*, Piscataaway, NJ, 2012, pp. 406-423.
[3] R. Tao, N. Zhang and Y. Wang, "Analysing and compensating the effects of range and doppler frequency migrations in linear frequency modulation pulse compression radar," *IET Radar Sonar Navig.*, vol. 5, no. 1, pp. 12-22, 2011.
[4] Z. Sun, X. Li, W. Yi, G. Cui and L. Kong, "Range walk correction and velocity estimation for high-speed target detection," in *Proc. IEEE Radar Conf.*, Seattle, WA, USA, May 2017, pp. 1478-1482.
[5] W. Wu, G. Wang and J. Sun, "Polynomial radon-polynomial fourier transform for near space hypersonic maneuvering target detection," *IEEE Trans. Aerosp. Electron. Syst.*, no. 99, pp. 1-16, Dec. 2017.
[6] G. Wang, J. Li, X. Zhang and W. Wu, "A tracking model for near space hypersonic slippage leap maneuvering target," *Acta Aeronautica et Astronautica Sinica (in Chinese)*, vol. 36, no. 7, pp. 2400-2410, Jul. 2015.
[7] M. Skolnik, "Role of radar in microwaves," *IEEE Trans. Microw. Theory Techn.*, vol. 50, no. 3, pp. 625-632, 2002.
[8] V. D. Julius and R. L. William, *Optimum radar detection*, 2nd ed. Raleigh, NC: Sci Tech, 2004.
[9] M. A. Richards, *Fundamentals of radar signal processing*, 2nd ed. New York, NY, USA: McGraw-Hill, 2014.
[10] D. C. Schleher, *MTI and pulsed doppler radar with MATLAB*, 2nd ed. Norwood, MA: Artech House, 2010.
[11] L. Cartledge and R. M. ODonnel, "Description and performance evaluation of the moving target detector," *Project Report ATC-69*, MIT Lincoln Laboratory, Mar. 1977.
[12] R. P. Perry, R. C. DiPietro, and R. L. Fante, "Coherent integration with range migration using keystone formatting," in *Proc. IEEE Radar Conf.*, Boston, MA, USA, Apr. 2007, pp. 863-868.
[13] D. Li, M. Zhan, H. Liu, Y. Liao and G. Liao, "A robust translational motion compensation method for ISAR imaging based on keystone transform and fractional fourier transform under low SNR environment," *IEEE Trans. Aerosp. Electron. Syst.*, vol. 53, no. 5, pp. 2140-2156, Mar. 2017.
[14] J. Xu, J. Yu, Y. Peng and X. Xia, "Radon-Fourier transform for radar target detection (I): Generalized doppler filter bank," *IEEE Trans. Aerosp. Electron. Syst.*, vol. 47, no. 2, pp. 1186-1202, Apr. 2011.
[15] J. Yu, J. Xu, Y. Peng and X. Xia, "Radon-Fourier transform for radar target detection (III): Optimality and fast implementations," *IEEE Trans. Aerosp. Electron. Syst.*, vol. 48, no. 2, pp. 991-1004, Apr. 2012.
[16] J. Xu, X. Zhou, L. Qian, X. Xia and T. Long, "Hybrid integration for highly maneuvering radar target detection based on generalized radon-fourier transform," *IEEE Trans. Aerosp. Electron. Syst.*, vol. 52, no. 5, pp. 2554-2561, Oct. 2016.
[17] X. Chen, J. Guan, N. Liu and Y. He, "Maneuvering target detection via Radon-Fractional Fourier transform-based long-time coherent integration," *IEEE Trans. Signal Process.*, vol. 62, no. 4, pp. 939-953, Feb. 2014.
[18] X. Chen, F. Cai, Y. Cong, J. Guan, "Radon-Fractional Fourier transform and its application to radar maneuvering target detection," in *Proc. Int. Radar Conf.* , Adelaide, SA, Australia, Sep. 2013, pp. 346-350.
[19] X. Lv, G. Bi, C. Wan and M. Xing, "Lv's distribution: Principle, implementation, properties, and performance," *IEEE Trans. Signal Process.*, vol. 59, no. 8, pp. 3576-3591, Aug. 2011.
[20] X. Li, G. Cui, W. Yi and L. Kong, "Coherent integration for maneuvering target detection based on Radon-Lvs distribution," *IEEE Signal Process. Letters*, vol. 22, no. 9, pp. 1467-1471, Sep. 2015.
[21] V. Namias, "The fractional order Fourier transform and its application to quantummechanics," *IMA J. Appl. Math*, vol. 25, no. 3, pp. 241-265, Feb. 1980.
[22] E. J. Kelly, I. S. Reed and W. L. Root, "The detection of radar echoes in noise," *J. SIAM*, vol. 8, pp. 309-341, Jun. 1960.
[23] R. J. Mcaulay and T. P. Mcgarty, "Maximum-likelihood detection of unresolved radar targets and multipath," *IEEE Trans. Aerosp. Electron. Syst.*, vol. AES-10, no. 6, pp. 821-829, Nov. 1974.
[24] S. Peleg and B. Friedlander, "The discrete polynomial-phase transform," *IEEE Trans. Signal Process.*, vol. 43, no. 8, pp. 1901-1914, Aug. 1995.
[25] B. D. Carlson, E. D. Evans and S. L. Wilson, "Search radar detection and track with the hough transform, Part I: System concept," *IEEE Trans. Aerosp. Electron. Syst.*, vol. 30, no. 1, pp. 102-108, Jan. 1994.

[26] J. Carretero-Moya, J. Gismero-Menoyo, A. Asensio-Lopez and A. Blanco-del-Campo, "A coherent Radon transform for small target detection," in *Proc. IEEE Radar Conf.*, Pasadena, CA, USA, May 2009, pp. 1-4.

[27] S. Buzzi, E. Grossi and M. Lops, "Dynamic programming techniques for sequential detection and tracking of moving targets in radar systems," in *Proc. 13th European Signal Process. Conf.*, Antalya, Turkey, Sep. 2009, pp. 1-4.

[28] A. F. Garcia-Fernandez, " Track-before-detect labeled multi-bernoulli particle filter with label switching," *IEEE Trans. Aerosp. Electron. Syst.*, vol. 52, no. 5, pp. 2123-2138, Oct. 2016.

[29] S. P. Ebenezer and A. Papandreou-Suppappola, "Generalized recursive track-before-detect with proposal partitioning for tracking varying number of multiple targets in low SNR," *IEEE Trans. Signal Process.*, vol. 64, no. 11, pp. 2819-2834, Jan. 2016.

[30] L. beda-Medina, . F. Garca-Fernndez and J. Grajal, "Adaptive auxiliary particle filter for track-before-detect with multiple targets," *IEEE Trans. Aerosp. Electron. Syst.*, vol. 53, no. 5, pp. 2317-2330, Apr. 2017.

[31] Z. Bai and J.W. Silverstein, *Spectral analysis of large dimensional random matrices*, 2nd ed. New York, NY, USA: Springer, 2010.

[32] J. Chen, F. Wang, and J. Zhou,"The metrication of LPI radar waveforms based on the asymptotic spectral distribution of Wigner matrices," in *Proc. IEEE Int. Symp. Inf. Theory*, Hong Kong, China, Jun. 2015, pp. 331-335.

[33] J. Chen, F. Wang, J. Zhou and C. Shi, "Spectral distribution of Wigner matrices in finite dimensions and its application to LPI performance evaluation of radar waveforms," *IEICE Trans. Fund. Elec. Com. Comput. Sci.*, vol. E100.A, no. 9, pp. 2021-2025, 2017.

[34] M. L. Mehta and M. Gaudin, "On the density of eigenvalues of a random matrix," *Nuclear Physics*, vol. 18, pp. 420-427, Aug. 1960.

[35] T. M. Cover and J. A. Thomas, *Elements of information theory*, 2nd ed. Hoboken, NJ: John Wiley & Sons, 2006.

[36] Z. Peng, X. Zhang, D. Li and X. Ji, "A study on accurate matched filtering and detection method of high-speed stealth target," *Modern Radar (in Chinese)*, vol. 39, no. 5, pp. 30-39, May 2017.

[37] S. K. Wong, E. Riseborough, G. Duff and K. K. Chan, "Radar cross-section measurements of a full-scale aircraft duct/engine structure," *IEEE Trans. Antennas Propag.*, vol. 54, no. 8, pp. 2436-2441, Aug. 2006.

[38] G. Blower, *Random matrices: high dimensional phenomena*, Cambridge, UK: Cambridge University Press, 2009.

[39] R. C. Dahiya and J. Gurland, "How many classes in the pearson chi-square test," *J. Am. Stat. Assoc.*, vol. 68, no. 343, pp. 707-712, Apr. 1973.

[40] R. J. Grissom and J. J. Kim, *Effect sizes for research: a broad practical approach*, Mahwah, NJ: Lawrence Erlbaum, 2005.

[41] Y. Zeng and Y. C. Liang, "Eigenvalue-based spectrum sensing algorithms for cognitive radio," *IEEE Trans. Commun.*, vol. 57, no. 6, pp. 1784-1793, Aug. 2009.

[42] E. H. G. Yousif, T. Ratnarajah and M. Sellathurai, "A frequency domain approach to eigenvalue-based detection with diversity reception and spectrum estimation," *IEEE Trans. Signal Process.*, vol. 64, no. 1, pp. 35-47, Jan. 2016.